*Radiophysics and Quantum Electronics, Vol. 47, Nos. 5–6, 2004*

# CHAOS AND HYPERCHAOS IN A BACKWARD-WAVE OSCILLATOR

**S. P. Kuznetsov** * **and D. I. Trubetskov**

UDC 517.9

*Based on a numerical solution of the equations of the nonstationary nonlinear theory, we study chaotic self-oscillation regimes in a backward-wave oscillator. For "weak" chaos, arising via a period-doubling cascade of self-modulation for moderate values of the normalized-length parameter, and for developed chaos, which corresponds to large values of this parameter, we present the temporal dependences of the output-signal amplitude, the phase portraits, and the statistical parameters of the dynamics. It is shown that developed chaos is characterized by the presence of more than one positive Lyapunov exponent (hyperchaos). We also present estimates of the Kolmogorov–Sinai entropy, the Lyapunov dimension, and the correlation dimension obtained from the Grassberger–Procaccia algorithm. The results confirm that a finite-dimensional strange attractor is responsible for the chaotic regimes in a backward-wave oscillator.*

## 1. INTRODUCTION

A backward-wave oscillator (BWO) is an electron device for generating electromagnetic oscillations of the microwave band. The idea of a BWO formed at the end of the forties — at the beginning of the fifties as a result of independent work of several research groups in the USSR (M. F. Stel'makh and collaborators), in England and the USA (R. Comfner, N. Williams, and J. Pierce), and in France (B. Epstein and collaborators). In a BWO, the electron beam interacts with the wave in a special electrodynamic system (slow-wave structure) under conditions where the phase velocity of the wave is close to the velocity of the electrons, while the group velocity is opposite in direction. Owing to the first condition, the electrons are subject to an efficient, accumulated action of the wave field, bunches are formed in the beam, and a high-frequency component of the current arises. Owing to the second condition, the energy of the radiation emitted by the bunches propagates toward the beam, which provides for internal feedback in the system and makes self-oscillations possible. In the "classical" variant of a backward-wave oscillator (O-type BWO), the electrons interact with the longitudinal component of the wave field, undergo displacements parallel to the beam axis (the bunching process) and transfer kinetic energy to the wave. Other variants of backward-wave systems, such as an M-type BWO, a BWO with transverse field, a relativistic BWO based on the anomalous Doppler effect, a gyro-BWO, a counterpropagating-wave peniotron, etc., are also known.

In the fifties and sixties, BWOs were intensely studied and developed for application in radar and communication systems, as master oscillators in transmitters and as local oscillators in fast-tunable receivers as well as in measurement engineering and radio spectroscopy. With the advent of high-efficiency, high-current accelerators in the seventies, it became possible to use the principle of backward-wave oscillation for creating powerful sources of electromagnetic radiation in the short-wavelength part of the microwave band based on relativistic electron beams.

* kuznetsov@sgu.ru

Saratov State University, Saratov Branch of the Institute of Radioengineering and Electronics, Saratov, Russia. Translated from Izvestiya Vysshikh Uchebnykh Zavedenii, Radiofizika, Vol. 47, Nos. 5–6, pp. 383–398, May–June, 2004. Original article submitted December 10, 2003.

0033-8443/04/4756-0341  

At the beginning of the seventies, studies aimed at developing the nonstationary nonlinear theory of backward-wave oscillators were conducted at the Saratov State University and at the Research Institute of Mechanics and Physics of the Saratov State University. In the monograph [1], which was published in 1975, the main principles of the nonstationary nonlinear theory of BWO were formulated, the theory of an M-type BWO was brought to a certain level of completion, and, in particular, the transient process, resulting in the onset of a stationary oscillation regime, was numerically simulated. The basic equations of the nonstationary theory of an O-type BWO were also formulated there, but their numerical solution was realized only some time later. Simultaneously, and independently, this was done during theoretical study of relativistic BWOs in Gorky (now Nizhny Novgorod) by M. I. Petelin group. According to the obtained results, the transient process in nonrelativistic or weakly relativistic BWOs leads to the onset of a stationary oscillation regime only if the operating current of the electron beam does not exceed the starting value, at which the oscillation begins, more than threefold. The larger electron-beam currents give rise to self-modulation regimes in which the signal amplitude at the BWO output oscillates in time either periodically or nonperiodically. After discussions at the Intercollegiate Conference on Microwave Electronics in Rostov-on-Don in autumn 1976, the effort of both groups was coordinated (see their collaborative papers [2–4]). The experiments conducted by B. P. Bezruchko confirmed the main results of the nonstationary theory. This concerns the occurrence of self-modulation and its characteristics such as the period and the spectrum as well as the experimentally obtained temporal dependences of the output-signal amplitude in the transient process [4–9]. Later, the results of the experiments with relativistic BWOs, in which self-modulation was also observed [10–12], were published. The influence of such factors as the space charge [8, 13–15], energy loss in the slow-wave structure [8, 15], end reflections of waves [16–20], and the external-signal forcing [8, 21, 22] on the BWO dynamics was examined.

One of fundamentally important results obtained in both the numerical calculations and the experiment was the discovery of chaotic oscillations in a BWO for fairly large dimensionless-length parameters, i. e., in the case where the operating current significantly exceeds the starting current [6–10]. In particular, such attributes of chaos as the continuous spectrum of an output signal and instability of the dynamics with respect to a small perturbation of the initial conditions were demonstrated. The scenario of chaos occurrence in a BWO was numerically studied in sufficient detail for the main theoretical model (see Eq. (1)) in [23, 24] and is briefly summarized in Sec. 2. It should be mentioned that in the actual BWOs, the dynamics in the domain of transition to chaos is strongly affected by additional factors (reflections, etc.) that are neglected in the basic model [16, 17, 19].

The detection of chaotic dynamics opens up an opportunity for using a BWO as a noise generator whose spectrum is concentrated in a certain frequency band and shifts over the range with the variation in the accelerating voltage [6–10, 25 ,26].

The present paper is devoted to a further study of chaotic self-oscillatory regimes in a backward-wave oscillator. In particular, we demonstrate the qualitative and quantitative difference between "weak" chaos, which is realized for moderate values of the normalized-length parameter, and developed chaos. The latter is characterized by the presence of more than one positive Lyapunov exponent, and should be classified as hyperchaos in terms of nonlinear dynamics. Estimates of the dimension of a strange attractor responsible for the chaotic regimes in a BWO are also presented.

## 2. EQUATIONS OF BWO DYNAMICS AND THE RESULTS OF THEIR SOLUTION. CASCADE OF ROUTE-TO-CHAOS BIFURCATIONS

The equations of the nonstationary theory of an O-type BWO in the simplest variant, without allowance for the space-charge effects, relativistic effects, and energy loss in the slow-wave structure (basic model) are written in the form

$$\partial^2\theta/\partial\zeta^2 = -\mathrm{Re}[F\exp(i\theta)], \qquad \partial F/\partial\tau - \partial F/\partial\zeta = -J, \qquad J = \frac{1}{\pi}\int\limits_0^{2\pi}\exp(-i\theta)\,\mathrm{d}\theta_0, \tag{1}$$

$$\theta|_{\zeta=0} = \theta_0, \qquad \partial\theta/\partial\zeta|_{\zeta=0} = 0, \qquad F|_{\zeta=L} = 0, \tag{2}$$

where the dimensionless independent variables $\zeta = \beta_0 C x$ and $\tau = \omega_0 C\,(t - x/v_0)\,(1 + v_0/v_{\rm gr})^{-1}$ are the coordinate and the "delayed" time, $v_0$ is the electron-beam velocity at the input of the interaction space, $v_{\rm gr}$ is the group velocity of the wave, $L = \beta_0 l C = 2\pi C N$ is the normalized length of the BWO, $l$ is the length of the system, $N$ is the number of slow waves on the system length, $C = \sqrt[3]{I_0 K_0/(4U)}$ is the Pierce parameter, which is assumed to be small, $I_0$ is the electron-beam current, $U$ is the accelerating voltage, and $K_0$ is the coupling impedance of the slow-wave structure. The quantity $\theta(\zeta, \tau, \theta_0)$ describes the phase of an electron, which entered the interaction space with the phase $\theta_0$, in the wave field, and the quantity $F(\zeta, \tau) = \tilde{E}/(2\beta_0 U C^2)$, the normalized complex amplitude of the high-frequency wave field $E(x,t) = {\rm Re}[\tilde{E}(x,t)\exp(i\omega_0 t - i\beta_0 x)]$.

It should be mentioned that equations (1) are universal in the sense that in a certain limiting case (small value of the product of the Lorentz factor squared and the interaction parameter in a relativistic BWO, ubitrons, and scattrons, large nonisochronism parameter in a gyro-BWO, etc.), these equations turn out to be identical (with accuracy up to normalization) for different electron devices with long-term backward-wave interaction based on the inertial mechanism of electron bunching [3].

Equations (1) and boundary conditions (2) specify the dynamic system with infinite-dimensional phase space. Indeed, for each fixed $\tau$, the field distribution over the coordinate $\zeta$ is described by a certain complex-valued function $F(\zeta)$. This function must be smooth, which is a natural requirement for the complex amplitude, and become zero at the right end of the system, which corresponds to $\zeta = L$. Since, as a result of solution of the equations, the field distribution $F(\zeta)$ is determined unambiguously for any $\tau' > \tau$, the set of admissible functions $F(\zeta)$ should be treated as the phase space of the system, where each point corresponds to a definite state of that system. When the state varies in time in accordance with equations (1), the representation point moves in the space of functions along a certain "phase trajectory."

The normalized length $L$ of the oscillator plays the role of the main control parameter, which is similar to the role which the Reynolds number plays in the analysis of turbulence. In practice, the parameter $L$ is usually chosen by specifying the electron-beam current $I_0$ which varies with the control-electrode voltage in the electron gun. In this case, $L \propto I_0^{1/3}$.

It is known that a stable equilibrium state $F \equiv 0$ is realized for small $L$. The fixed point looses its stability if $L = L_{\rm st} = 1.97327$. A numerical solution of Eqs. (1) shows that for $L_{\rm st} < L < L_{\rm AM} \approx 2.937$ the transient process ends with the onset of a stationary oscillation regime. The amplitude of an output signal is stabilized at a certain level and is not changed with time, and the frequency, i. e., the rate of phase variation of the complex variable $F$, also becomes constant [2–5].

For $L > L_{\rm SM}$, there occurs self-modulation, i. e., self-sustained oscillations of the output-signal amplitude with a characteristic period determined by the time $T_{\rm SM} \propto 1.5\,(l/v_0 + l/v_{\rm gr})$ [2–5] of passage of a signal over the feedback loop [2–5]. The bifurcation diagram taken from [23, 24] and shown in Fig. 1*a* gives an idea of the further sequence of transitions. The "simple" self-modulation regimes discussed above are shown by a separate line near the left edge of the diagram. For $L = L_1 \approx 4.0$, this line bifurcates, which corresponds to a period-doubling bifurcation of self-modulation (the form of self-modulation "spikes" is repeated every second time). Then further period-doubling bifurcations of self-modulation for $L = L_2, L_3, \ldots$ and a transition to chaos take place in a narrow region of variation in the parameter $L$. A close-up of the corresponding fragment of bifurcation diagram is given in Fig. 1*b*. With accuracy up to fine detail, this fragment reproduces the pattern known for a wide class of nonlinear dissipative systems as Feigenbaum's scenario of transition to chaos via an infinite cascade of period-doubling bifurcations. The limiting point of this sequence, i. e., Feigenbaum's critical point, corresponds to the threshold of chaos occurrence. In the supercritical region, one can see chaos areas and periodicity windows (for example, windows of periods 5 and 7 are clearly seen). Universal quantitative relationships inherent in Feigenbaum's scenario [27–29] hold near the critical point.[1]

[1] From the formal viewpoint, periodic self-modulation corresponds to a torus, not a cycle, in the phase space of the initial

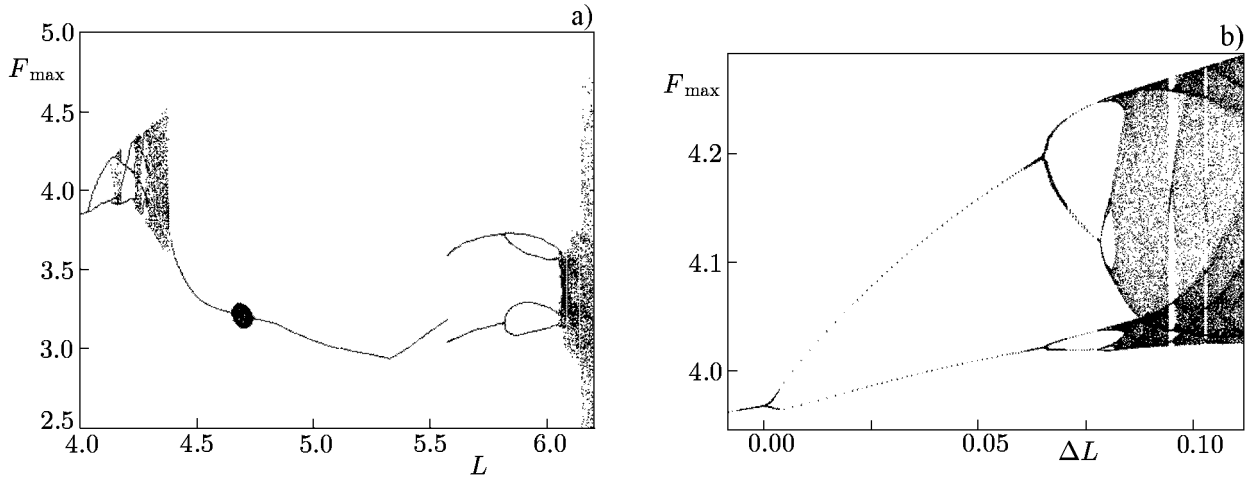


Fig. 1. Bifurcation diagram of the BWO model, described by Eqs. (1) and (2), from [23, 24] (*a*). The horizontal axis is the normalized length $L$, and the vertical axis is the maximum values of the output-signal amplitude, which are reached in the stationary regime. A fragment of the bifurcation diagram corresponding to the region of transition to chaos via a period-doubling cascade of self-modulation (*b*). The horizontal axis is the quantity $\Delta L = L - L_1$, where $L_1 \approx 4.0$ corresponds to the first period-doubling bifurcation.

It appears that chaos resulting from a period-doubling cascade of self-modulation is, in a certain sense, undeveloped, "weak." Firstly, this chaos exists only for a narrow interval of values of the parameter $L$. Secondly, the temporal dependence of the amplitude looks like an approximate repetition of "spikes" of similar shape and size in about the same intervals of time, while the intensity of the noise component in the spectrum is fairly small. The spatial distribution of the field does not show the rich variety in form which should be typical of developed chaos, i. e., "turbulence."

The region of period doublings of self-modulation is followed by a large number of periodicity windows in the interval $4.15 < L < 4.33$. The further increase in the parameter $L$ is accompanied by a transition from chaotic to periodic self-modulation via type-I Pomeau–Manneville intermittency [29, 30]. As a result, chaotic self-modulation is replaced by periodic for $L \approx 4.33$. Then the self-modulation becomes quasi-periodic (in an interval of about from 4.6 to 4.75) and after that becomes periodic again. Obviously, a strange attractor in the phase space transforms to a metastable chaotic set. The transient process, preceding the onset of a regular self-modulation regime, must take a long time which exceeds significantly the typical self-modulation period.

Finally, for sufficiently large values of $L \gtrsim 6$, which correspond to electron-beam currents exceeding the starting current by a factor of 30 or more, the temporal variations in the signal amplitude and phase become obviously irregular, chaotic. No trend toward the onset of a regime with constant or periodically varied amplitude is observed even during a very large time. However, the squared amplitude $|F|^2$ and the rate of variation in the signal phase, averaged over a time $\tau$ of the order of unity, become approximately constant. Hence, it is expedient that the corresponding regime be regarded steady-state. The regime with

system. It is well known in nonlinear dynamics that, unlike the cycle-doubling sequence, the torus-doubling sequence typically contains a finite number of bifurcations. Nevertheless, a complete period-doubling cascade of self-modulation obviously takes place in our BWO model. In fact, the considered equations have the specific symmetry, i. e., are invariant with respect to phase shifts. Hence, our BWO model cannot be regarded as belonging to the class of typical systems in the context of bifurcation analysis. Indeed, owing to the mentioned invariance, the problem can be formulated such that the variable responsible for the output-signal phase is excluded from consideration. For this, it suffices to introduce the new variable $\tilde{F}(\tau) = F(\tau)\exp[-i\arg(F(\tau, 0))]$ instead of $F(\tau, \zeta)$, although in this case, the corresponding form of the equations is less convenient. Then from the two-dimensional torus, corresponding to the periodic self-modulation regime, we return to the limit cycle which can undergo an infinite period-doubling sequence. Outside the framework of the method of slowly varying amplitudes, this argument is no longer valid, and, obviously, either a finite torus-doubling sequence or period-doubling cascades based on periodic regimes corresponding to the resonance cycles on a torus will be realized.

the same statistical parameters also arises under other initial conditions and should therefore be qualified as chaotic self-oscillations.

## 3. "WEAK" CHAOS AND DEVELOPED CHAOS IN THE BWO DYNAMICS. PHENOMENOLOGY AND THE STATISTICAL PARAMETERS

For a detailed analysis, we choose two regimes which are observed in the basic BWO model for the normalized length $L = 4.24$ ("weak" chaos) and $L = 6.1$ (developed chaos). Figure 2 shows the temporal dependences of the output-signal amplitude after a time about a hundred of typical periods of amplitude oscillations from the beginning of the process.

Figure 3 presents the phase portraits (two-dimensional projections of strange attractors) obtained by the Takens method from the signal amplitude observed at the BWO output. The coordinate axes are the output-signal amplitudes at the current and delayed instants of time. In the case of weak chaos, the phase portrait demonstrates a visually discernible fine structure, which is qualitative evidence for a small dimension of the strange attractor. In the second case, such a structure is not seen, which is indicative of a considerably larger dimension.

Figure 4 shows the distribution of the mean square $\sigma^2(\zeta) = \overline{|F(\tau,\zeta)|^2}$ of the field amplitude over the system length and the root-mean-square deviation $\kappa(\zeta) = \sqrt{\overline{|F(\tau,\zeta)|^4 - (\overline{|F(\tau,\zeta)|}^2)^2}}$ of this quantity, where the overbar denotes averaging over time. The quantity $\sigma^2(\zeta)$ specifies the average energy flux of an electromagnetic wave in the given cross section $\zeta$ of the system, and $\kappa(\zeta)$ describes fluctuations in the energy flux. It is seen that both quantities increase monotonically from zero to the maximum from the right to the left along the interaction space. In the weak-chaos regime, $\kappa(\zeta)$ is greater than $\sigma^2(\zeta)$, which is related to the presence of an intense, almost periodic component in the dynamics of the system. Note that the relationship is inverse for developed chaos.

Figure 5 shows the plots of the distribution function $f(|F|)$ of the output-signal amplitude. For weak chaos, this function has a characteristic form with a number of peaks associated with the most probable values of the minima and maxima of the output-signal amplitude, which are realized with fairly correct regularity. In the developed-chaos regime, the distribution function is smooth and has one pronounced maximum. With the further increase in the parameter $L$, the distribution function approaches the Rayleigh function typical of the case where the complex amplitude of the output signal is a random process with a Gaussian distribution of the real and imaginary parts.

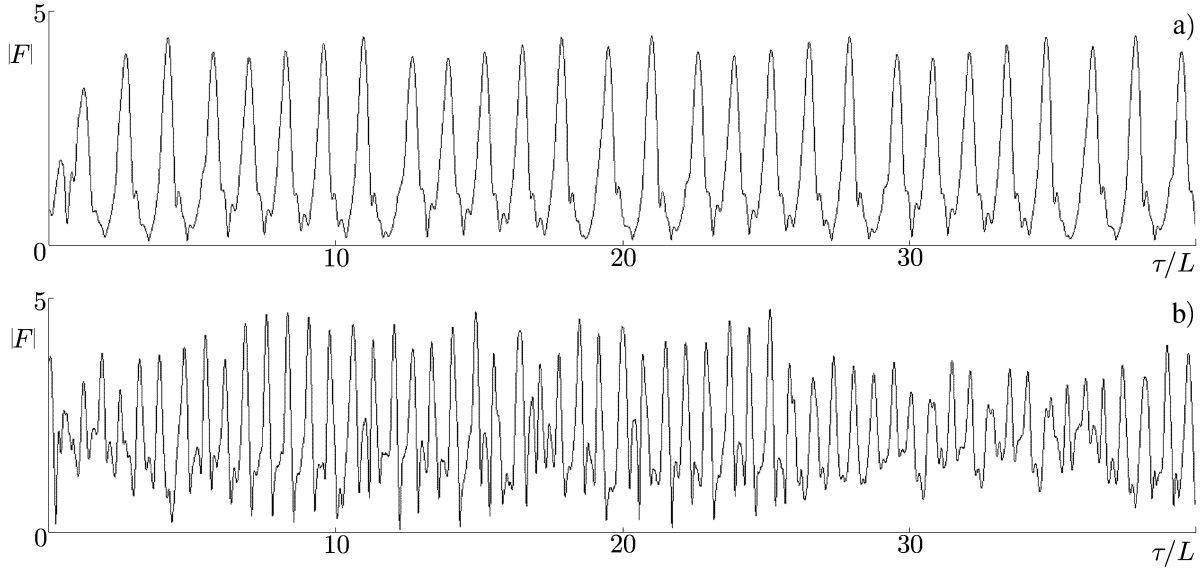


Fig. 2. Temporal dependences of the output-signal amplitude of a BWO after the transient process is over, which are based on the results of numerical solution of Eqs. (1) and (2) for $L = 4.24$ (*a*) and $L = 6.1$ (*b*).

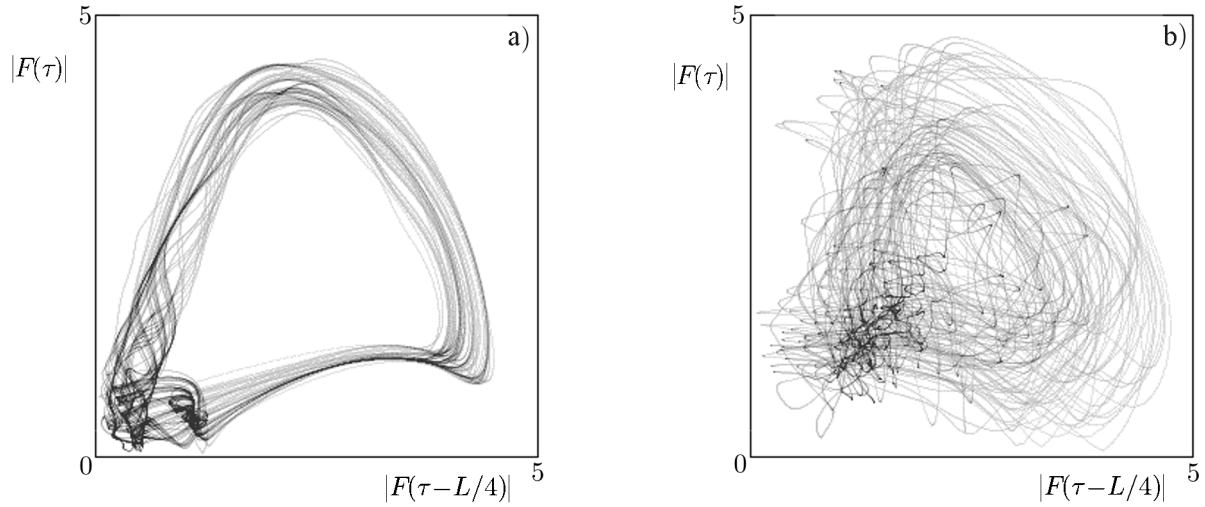


Fig. 3. Phase portraits of weak chaos for $L = 4.24$ (*a*) and developed chaos for $L = 6.1$ (*b*).

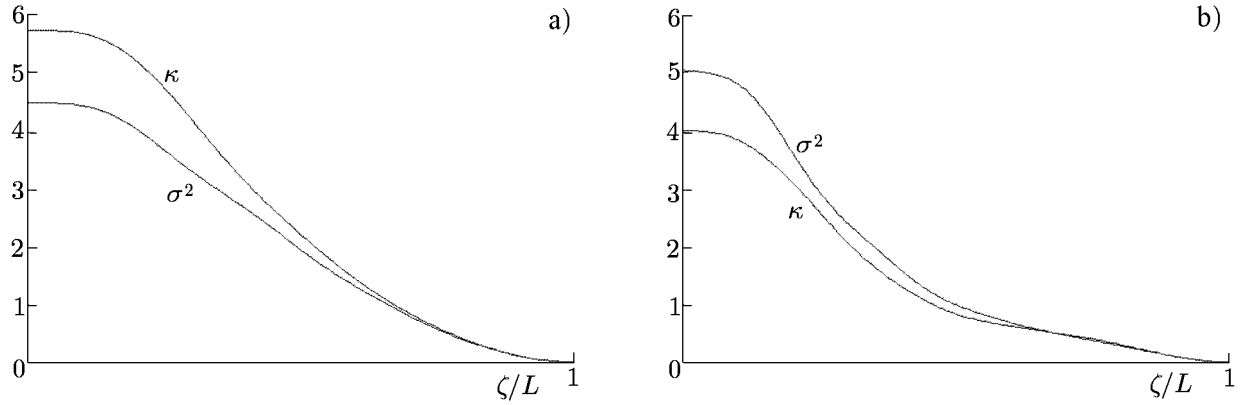


Fig. 4. Distribution of the mean square $\sigma^2(\zeta)$ of the field amplitude, which characterizes the average energy flux of the wave, and of the root-mean-square deviation $\kappa(\zeta)$ of this quantity, which characterizes energy-flux fluctuations, over the system length in the regimes of weak chaos for $L = 4.24$ (*a*) and developed chaos for $L = 6.1$ (*b*).

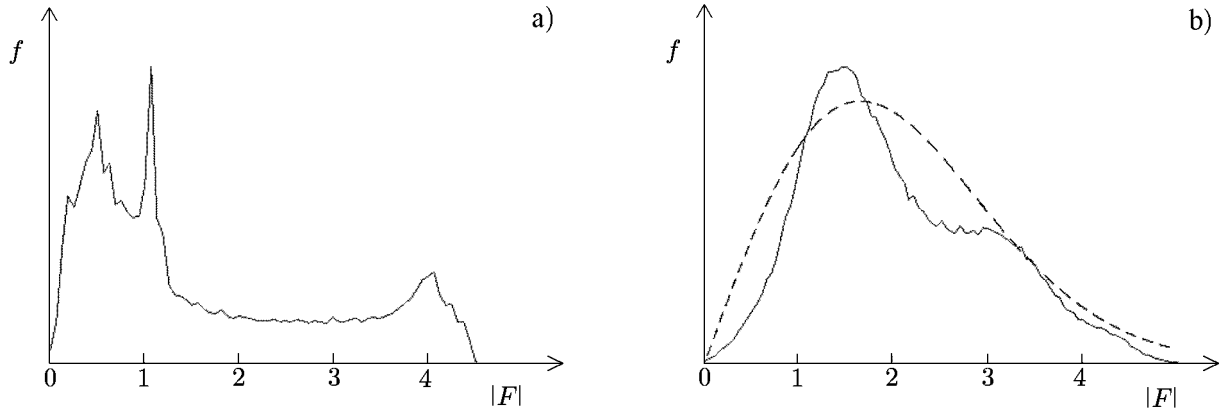


Fig. 5. Distribution function of the dimensionless amplitude of the output signal, obtained on the basis of numerical solution of Eqs. (1) and (2) in the regimes of weak chaos for $L = 4.24$ (*a*) and developed chaos for $L = 6.1$ (*b*). The dashed line shows the Rayleigh distribution function corresponding to a random signal whose real and imaginary parts of the complex amplitude have the Gaussian distribution.

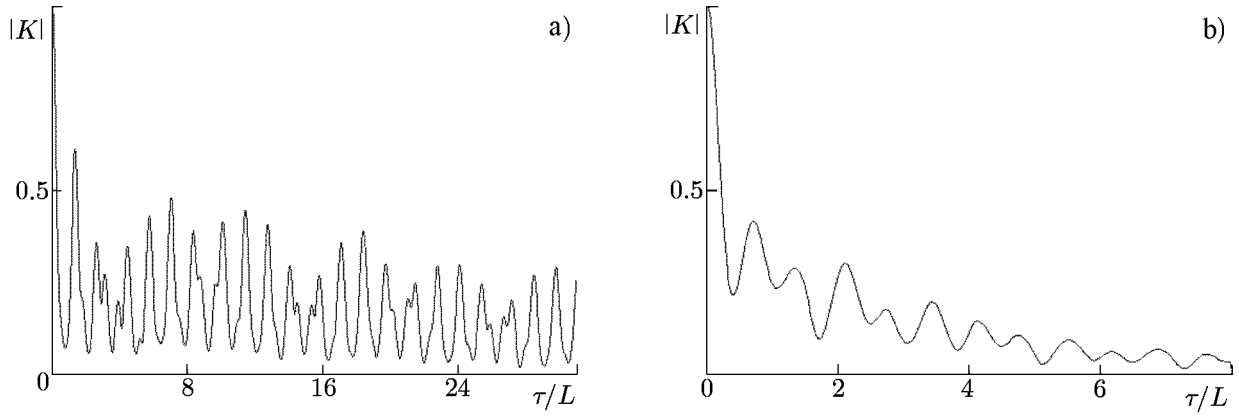


Fig. 6. Autocorrelation function of the output signal obtained from the results of numerical simulation of Eqs. (1) and (2) in the regimes of weak chaos for $L = 4.24$ (*a*) and developed chaos for $L = 6.1$ (*b*).

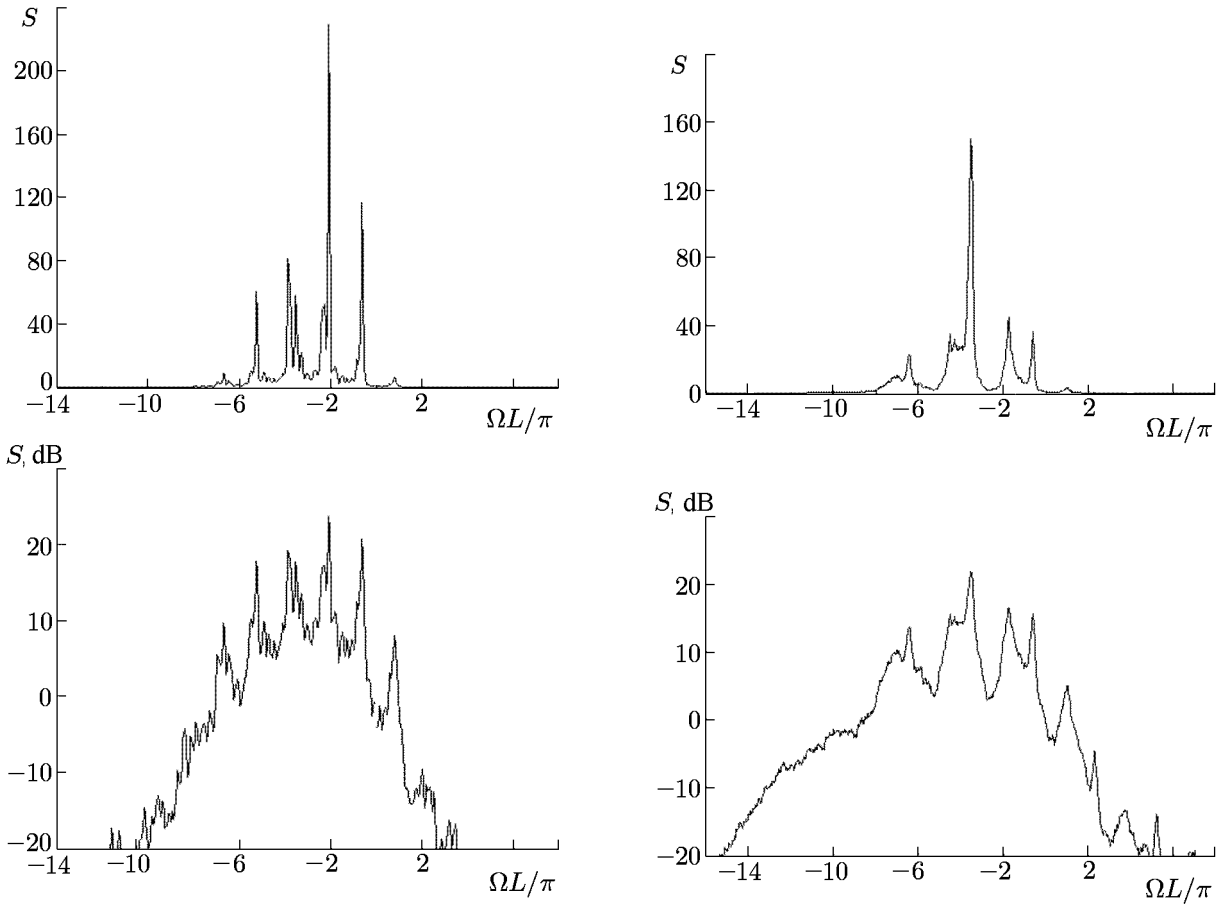


Fig. 7. Power spectra of the output signal of a BWO obtained from the results of numerical simulation of Eqs. (1) and (2) in the regimes of weak chaos for $L = 4.24$ (left) and developed chaos for $L = 6.1$ (right). The spectrum is shown in quadratic scale in the upper plots and in logarithmic scale in the lower plots.

Figure 6 shows the magnitude of the autocorrelation function

$$K(T) = \overline{F(\tau,0)F^*(\tau+T,0)}/\overline{|F(\tau,0)|^2} \tag{3}$$

of the output radiation of a BWO for the cases of weak and developed chaos. As is known, chaotic regimes are characterized by the disappearance of correlation between parts of a realization which are well separated

in time, i. e., $K(T) \to 0$ for $T \to \infty$. It is seen in Fig. 6 that in the developed-chaos regime, the correlation function indeed decreases rapidly, while oscillating as the parameter $T$ increases. The oscillations decrease much slower in the case of weak chaos.

According to the Wiener–Khinchin theorem, the Fourier image of the autocorrelation function gives the power spectral density of a signal, and turns out to be continuous if $K(T) \to 0$.

Figure 7 presents the power spectra of the output signal of a BWO in the regimes of weak and developed chaos. To construct the spectra, according to the theory of numerical spectral analysis of random processes, the available realization was divided into segments of length $T_0$ (the quantity $\Delta\omega = \pi/T_0$ specifies the resolution of analysis), the result was multiplied by the function $\sin^2(\pi\tau/T_0)$ (the so-called "window") in each segment, then the Fourier transform was performed, and finally the result was averaged over all the segments. The larger the number of available segments, the smaller the rms error of the estimate of the power spectral density. The spectra are represented in quadratic and logarithmic scales. The first one permits visual estimation of the actual distribution of power over the spectrum, and the second one highlights fine-structure details of the spectrum.

It is clearly seen in the logarithmic plots that in both considered regimes, the spectrum is continuous. In this respect, it is similar to the spectrum of a stationary random process. It should be mentioned that the spectrum comprises high "peaks," which are especially pronounced in the case of weak chaos. In the developed-chaos regimes, these peaks become the smoother, the larger is the parameter $L$.

## 4. PROPERTIES OF THE SENSITIVITY OF THE DYNAMICS TO INITIAL-CONDITION PERTURBATIONS. THE LYAPUNOV EXPONENTS

As is known, the instability of phase trajectories, or high sensitivity of motion to small variations in the initial conditions, is one of the main attributes of dynamic chaos. We will demonstrate that this property is present in the dynamics of a BWO. Let us choose the normalized length of the oscillator corresponding to the chaotic regime, specify the initial conditions in the form of a certain distribution of a small-amplitude field with a small random addition, solve Eqs. (1) and (2) numerically many times, and represent the set of obtained realizations, i. e., temporal dependences of the output-signal amplitude, in one diagram.

Figure 8 shows the results of numerical calculations, obtained in such a way, for the regimes of weak chaos for $L = 4.24$ and developed chaos for $L = 6.1$. It is seen that in the initial section, the realizations repeat each other, but diverge increasingly stronger with time as the right edge of the diagram is approached, so that the picture becomes smear. The performed numerical experiment is similar to the actual experiment described in [7–9].

As is known, the Lyapunov exponents, which determine the exponential (on the average) growth or decay of perturbations near the typical phase trajectory belonging to the strange attractor, are used as the qualitative characteristics of the phase-trajectory instability inherent in chaos. In this case, the total number of Lyapunov exponents corresponds to the dimension of the phase space of the studied system. The existence of at least one positive Lyapunov exponent of an attractor is the criterion of chaos. The case where more than one exponent are positive is called hyperchaos.

In our case, the phase space of the system given by Eqs. (1) and (2) is infinite-dimensional, and the total number of Lyapunov exponents must be infinite. In [8, 9], Bezruchko et al. considered the procedure (the Benettin algorithm adapted in an appropriate way) [29, 31] for calculating the maximum exponent. Here, we intend to improve this procedure by analogy with [29, 32] so as to obtain several largest Lyapunov exponents from their total spectrum. In particular, this permits one to differentiate between "simple" chaos and hyperchaos as well as obtain data for estimating the fractal dimension of the attractor using the Kaplan–Yorke formula.

Introducing Lyapunov exponents, it is convenient to use the ratio $\tau/L$ of the normalized time to the normalized length of the oscillator and assume that the evolution of a perturbation is described by the expression $\tilde{F} \propto \exp(\Lambda\tau/L)$. With such a definition, the normalization of the dimensionless Lyapunov exponent $\Lambda$ turns out to be independent of the electron-beam current.

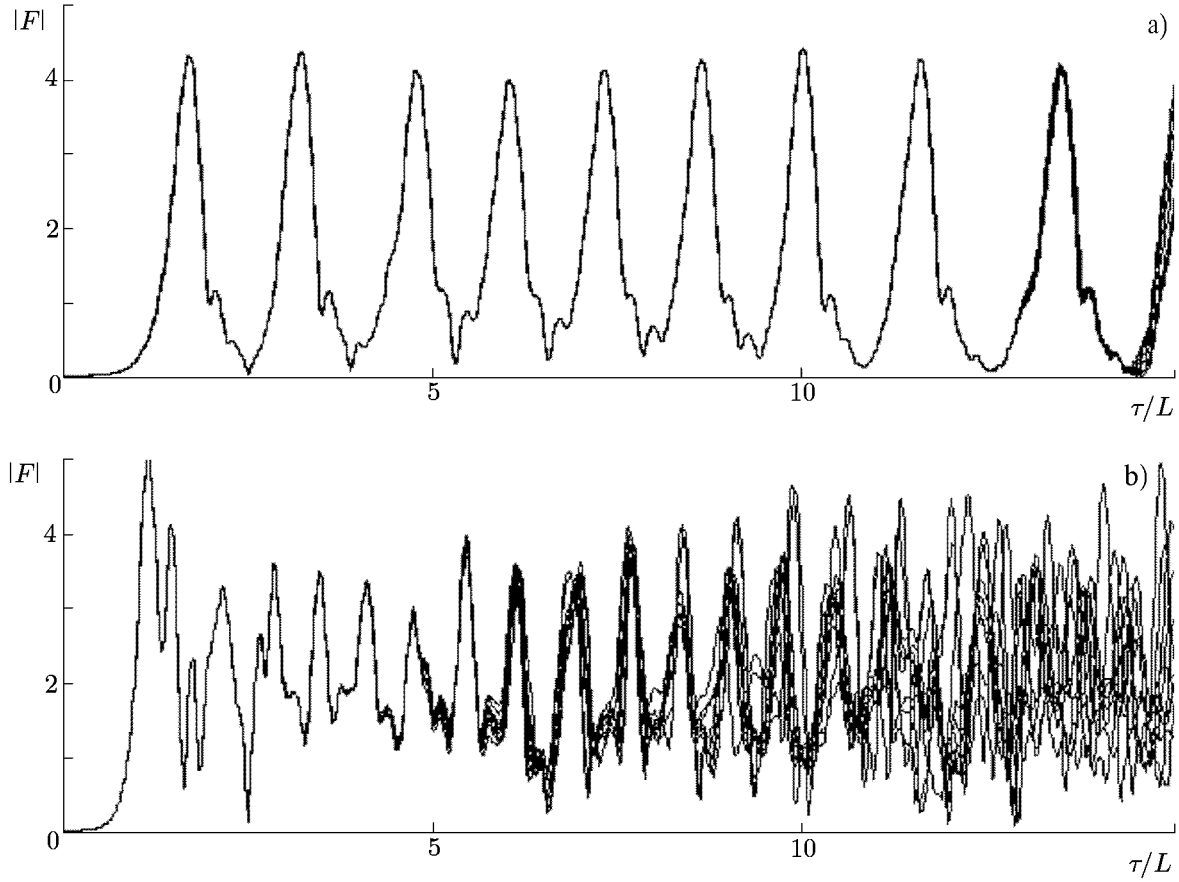


Fig. 8. Illustration of the sensitivity of the BWO dynamics to a small perturbation of the initial conditions in the numerical experiment for $L = 4.24$ (*a*) and $L = 6.1$ (*b*). Each diagram represents 20 temporal dependences of the output-signal amplitude. The field-amplitude distribution at the level 0.01 with a random addition of the order of 0.001 was used as the initial conditions.

For the numerical calculation of $n$ Lyapunov exponents, we consider $n + 1$ samples of the system described by Eqs. (1) and (2). Let the field-amplitude distribution at the initial time $\tau_0$ in the system with number $k = 0$ be specified by the complex-valued function $F(\zeta)$, and in other cases, by the functions $F_k(\zeta) = F(\zeta) + \varepsilon\tilde{F}_k(\zeta)$, where $\|\tilde{F}_k\| = \int_0^1 |\tilde{F}_k|^2\,\mathrm{d}\zeta = 1$ and $\varepsilon \le 1$, $k = 1, 2, \ldots, n$. Solving numerically $n + 1$ systems of equations for the nonstationary boundary-value problem, we obtain a new set of functions $\tilde{F}_k(\zeta) = [F_k(\zeta) - F(\zeta)]/\varepsilon$ at the next instant of time $\tau_1 = \tau_0 + \Delta\tau$. In this case, the interval $\Delta\tau$ is chosen fairly small to ensure that perturbations of the norm remain small. Following the Gram–Schmidt method, we use the relationships

$$\begin{gathered}
\tilde{F}_1^0 = \tilde{F}_1/\|\tilde{F}_1\|, \qquad \tilde{F}_2' = \tilde{F}_2 - (\tilde{F}_2, \tilde{F}_1^0)\,\tilde{F}_1^0, \qquad \tilde{F}_2^0 = \tilde{F}_2'/\|\tilde{F}_2'\|, \\
\tilde{F}_3' = \tilde{F}_3 - (\tilde{F}_3, \tilde{F}_1^0)\,\tilde{F}_1^0 - (\tilde{F}_3, \tilde{F}_2^0)\,\tilde{F}_2^0, \qquad \tilde{F}_3^0 = \tilde{F}_3'/\|\tilde{F}_3'\|, \\
\tilde{F}_4' = \tilde{F}_4 - (\tilde{F}_4, \tilde{F}_1^0)\,\tilde{F}_1^0 - (\tilde{F}_4, \tilde{F}_2^0)\,\tilde{F}_2^0 - (\tilde{F}_4, \tilde{F}_3^0)\,\tilde{F}_3^0, \qquad \tilde{F}_4^0 = \tilde{F}_4'/\|\tilde{F}_4'\|, \\
\ldots
\end{gathered} \tag{4}$$

to perform orthogonalization and renormalization of the perturbation vectors. Here, the parentheses stand for the scalar product: $(f, g) = \int_0^1 f(\zeta)g^*(\zeta)\,\mathrm{d}\zeta$. Then we continue calculations at the next "step" of the algorithm of duration $\Delta\tau$ with newly determined perturbations

$$F_m(\zeta) \leftarrow F_m(\zeta) + \varepsilon\tilde{F}_m^0(\zeta). \tag{5}$$

The whole procedure is repeated many times during a large number of "steps." The product $\prod_{k=1}^{M_0} \|\tilde{F}_m\|_{\tau=k\Delta\tau}$ yields the factor by which the norm of the $m$th perturbation vector is changed in the linear approximation after $M_0$ steps of the algorithm, and the corresponding Lyapunov exponent is expressed in terms of the logarithm of this quantity:

$$\Lambda_m = S_m\,(M_0\,\Delta\tau)/(M_0 L\,\Delta\tau), \qquad S_m = \sum_{k=1}^{M_0} \ln \|\tilde{F}_m\|_{\tau=k\Delta\tau}. \tag{6}$$

As far as the spectrum of the Lyapunov exponents is concerned, it is useful to bear in mind that any attractor in our system, different from a trivial fixed point, has two zero exponents. This is related to the fact that, since the equations of the nonstationary theory of a BWO are invariant with respect to two types of infinitesimal shifts (both in time and in phase), perturbations of the form

$$\tilde{F}_\tau(\zeta,\tau) \equiv \partial F(\zeta,\tau)/\partial\tau \qquad \text{and} \qquad \tilde{F}_\varphi(\zeta,\tau) \equiv iF(\zeta,\tau) \tag{7}$$

neither increase nor decrease with time (on the average) during evolution of the system state. Therefore, these perturbations correspond to the zero Lyapunov exponents. The accuracy of estimation of other exponents considerably increases if terms given by Eq. (7) are excluded from the considered perturbation vector at each "step" of the algorithm during the calculation:

$$\tilde{F}(\zeta) \leftarrow \tilde{F}(\zeta) - c_1\tilde{F}_\tau - c_2\tilde{F}_\varphi. \tag{8}$$

Here, $c_1 = (\tilde{F},\tilde{F}_\tau)/\|\tilde{F}_\tau\|$ and $c_2 = (\tilde{F},\tilde{F}_\varphi)/\|\tilde{F}_\varphi\|$ are the complex coefficients minimizing the perturbation norm.

Figure 9 gives typical diagrams of the dependence of the "accumulated sums" $S_m = \Sigma_{k=1}^{M_0} \ln \|\tilde{F}_m\|_{\tau=k\Delta\tau}$ on the normalized time during calculation of two nonzero Lyapunov exponents in the regime of weak chaos for $L = 4.24$ and five exponents in the regime of developed chaos for $L = 6.1$. The estimate of the Lyapunov exponents is given by the angular coefficients of the straight lines approximating these dependences. Table 1 gives a summary of the Lyapunov exponents obtained by processing of ten such diagrams and arranged in the decreasing order (two zero exponents, whose existence follows from the invariance of the equations with respect to temporal and phase shifts, are added to them). In the first case, the Lyapunov-exponent spectrum of a chaotic attractor has the signature $\langle +, 0, 0, -, \ldots\rangle$, i. e., low-dimensional chaos with one positive Lyapunov exponent takes place. In the second case, which corresponds to hyperchaos, there are two positive exponents: $\langle +, +, 0, 0, -, \ldots\rangle$.

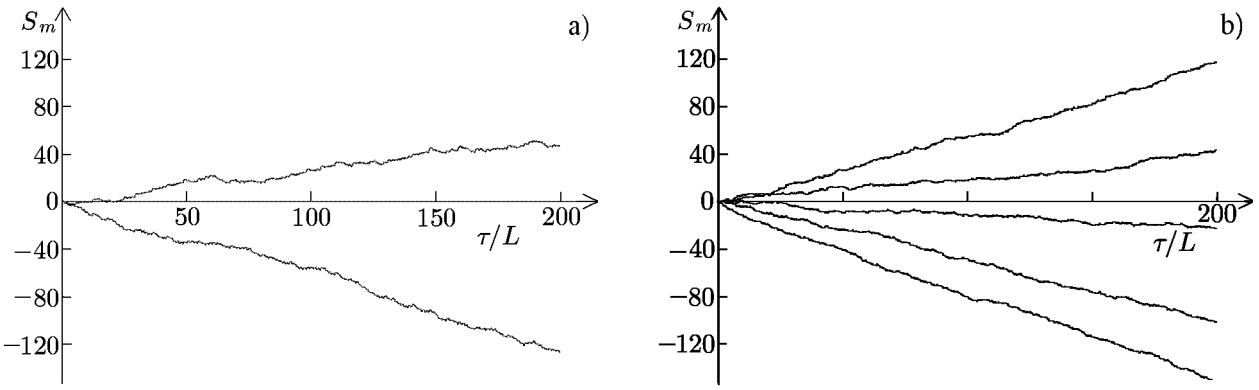


Fig. 9. Typical diagrams of the dependence of the "accumulated sums" on the normalized time during calculation of two nonzero Lyapunov exponents using generalized Benettin's algorithm in the regime of weak chaos for $L = 4.24$ and five exponents in the regime of developed chaos for $L = 6.1$. The estimate of the Lyapunov exponents is given by the angular coefficients of the straight lines approximating these dependences.

TABLE 1. The Lyapunov exponents and the related quantities obtained in the numerical calculations for the basic BWO model.

| | Lyapunov exponents | Spectrum signature | Kolmogorov–Sinai entropy | Lyapunov dimension |
|---|---|---|---|---|
| Weak chaos, $L = 4.24$ | $\Lambda_1 = 0.268 \pm 0.010$<br>$\Lambda_2 = \Lambda_3 = 0$<br>$\Lambda_4 = -0.593 \pm 0.006$ | $\langle +, 0, 0, -, \ldots \rangle$ | $h = \Lambda_1 = 0.268$ | $D_{\mathrm{L}} = 3.45$ |
| Developed chaos (hyperchaos), $L = 6.1$ | $\Lambda_1 = 0.594 \pm 0.006$<br>$\Lambda_2 = 0.254 \pm 0.003$<br>$\Lambda_3 = \Lambda_4 = 0$<br>$\Lambda_5 = -0.093 \pm 0.010$<br>$\Lambda_6 = -0.449 \pm 0.020$<br>$\Lambda_7 = -0.803 \pm 0.005$ | $\langle +, +, 0, 0, -, -, -, \ldots \rangle$ | $h = \Lambda_1 + \Lambda_2 = 0.848$ | $D_{\mathrm{L}} = 6.38$ |

Table 1 also includes other characteristics of two considered chaotic regimes, which can be obtained on the basis of the Lyapunov exponent spectrum. In particular, the sum of positive Lyapunov exponents yields the estimate of the Kolmogorov–Sinai entropy which indicates how information produced by the system during motion over the chaotic attractor increases with time. Another characteristic is the dimension of the attractor obtained using the Kaplan–Yorke formula

$$D_{\mathrm{L}} = M + \left( \sum_{i=1}^{M} \Lambda_i \right) \Big/ |\Lambda_{M+1}|, \tag{9}$$

where $M$ is an integer for which $S_M = \Sigma_{i=1}^{M} \Lambda_i > 0$, but $S_{M+1} = \Sigma_{i=1}^{M+1} \Lambda_i < 0$. In practice, this formula usually gives an accurate estimate of the fractal dimension of a strange attractor. The dimension calculated using Eq. (9) is generally referred to as the Lyapunov dimension. In our case, the Lyapunov dimension equals 3.45 in the regime of weak chaos and 6.38 in the regime of hyperchaos.

It is useful to plot the dependence of the sum $\Sigma_m = \Sigma_{i=1}^{m} \Lambda_i$ of the Lyapunov exponents on the number of terms by connecting the points by a broken line (Fig. 10). This diagram gives the idea of a relationship

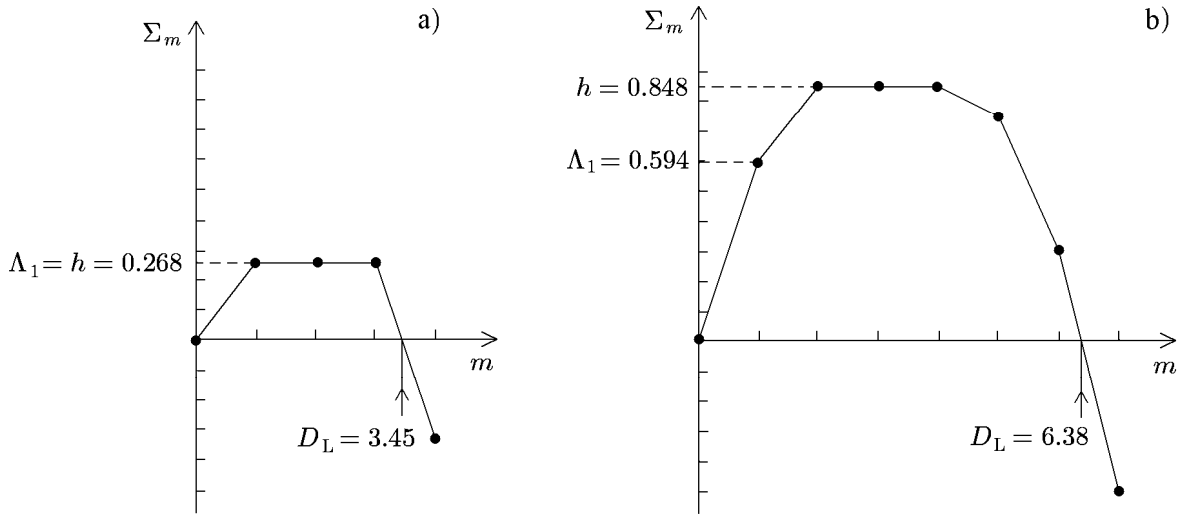


Fig. 10. Dependence of the sum of several first Lyapunov exponents on the number of terms in the cases of weak chaos for $L = 4.24$ (*a*) and developed chaos for $L = 6.1$ (*b*). The diagrams show the maximum Lyapunov exponent $\Lambda_1$, the Kolmogorov–Sinai entropy, and the Lyapunov dimension $D_{\mathrm{L}}$ based on the Kaplan–Yorke formula.

among several characteristics of the attractor that are important for the nonlinear dynamics. In particular, the quantity $\Sigma_1$, obtained for $m = 1$, is the maximum Lyapunov exponent $\Lambda_1$, and the maximum value of $\Sigma_m$ corresponds to the Kolmogorov–Sinai entropy. The point of intersection of the diagram and the horizontal axis corresponds to the dimension $D_{\mathrm{L}}$ calculated using the Kaplan–Yorke formula.

## 5. CORRELATION DIMENSION OF THE ATTRACTOR

Calculation of the Grassberger–Procaccia correlation dimension for the attractor reconstructed by the Takens method is one of the most popular procedures of estimating qualitative characteristics of chaos in nonlinear dynamics and its applications.

In our system, the scalar time series for the subsequent processing was obtained from a numerical solution of nonstationary nonlinear equations (1) and (2) by sampling the values of the squared amplitude of the output signal with a definite time step $\tau_0$ which usually amounted to several steps of the difference scheme:

$$x_0 = |F(0,0)|^2, \qquad x_1 = |F(\tau_0,0)|^2, \qquad x_2 = |F(2\tau_0,0)|^2, \qquad x_3 = |F(3\tau_0,0)|^2, \qquad \ldots . \tag{10}$$

Assign a certain integer $m$ and construct a sequence of vectors in a space of dimension $m$, assuming

$$\mathbf{x}_i = (x_i, x_{i-p}, x_{i-2p}, \ldots, x_{i-(m-1)p}). \tag{11}$$

Here, $i = 1, 2, \ldots, P$ and $p$ is an integer which should reasonably be selected such that to improve at best the obtained result.

Considering the set of points $\mathbf{x}_i$, it is possible to estimate its dimension using the Grassberger–Procaccia method. To do this, one should calculate the so-called correlation integral

$$C(\varepsilon) = \lim_{P\to\infty} \frac{1}{P\,(P-1)} \sum_{i,j=1}^{P} \theta(\varepsilon - \|\mathbf{x}_i - \mathbf{x}_j\|) \tag{12}$$

as a function of $\varepsilon$. The resulting dependence on a log–log plot has a linear region (scaling region), and the angular coefficient (slope) $D(m)$ in this region yields an estimate of the dimension of the attractor's projection onto $m$-dimensional space.

The described procedure is sequentially performed several times for $m = 1, 2, 3, \ldots$. The presence or absence of saturation of the dependence $D(m)$ with increasing $m$ is considered a criterion showing whether the signal is generated by the dynamic system or is noisy. If saturation is observed at a certain level $D$, then this value is taken as an estimate for the correlation dimension of the attractor of the dynamic system that generated the observed signal.

Consider the use of such an approach for processing of a time series obtained by numerical solution of nonstationary BWO equations in the regimes of weak chaos for $L = 4.24$ and developed chaos for $L = 6.1$.

Figure 11 shows the dependences of the correlation integral on $\varepsilon$ and on the embedding dimension $m$. In the region where the diagram is approximated by a straight line, its slope with increasing $m$ has the trend toward saturation for two considered regimes at the levels $D_2 \approx 2.3$ and $D_2 \approx 5.8$, respectively. Since the phase variable was neglected for the adopted definition of the time series, the actual correlation dimension of the attractor is by one larger and should be considered equal to $D_2 \approx 3.3$ and $D_2 \approx 6.8$, respectively. This is in reasonable agreement with the above-obtained estimates of the Lyapunov dimension ($D_{\mathrm{L}} \approx 3.45$ and $D_{\mathrm{L}} \approx 6.38$, respectively). The fractional value of the dimension is an additional indication that we deal with a strange attractor. The finite value of the dimension indicates that actually a finite (not very large) number of degrees of freedom are involved in the considered regimes of dynamics of a distributed system. Indeed, in accordance with Mane's theorem, the dimension of the phase space in which the attractor is embedded does not exceed the value $2D + 1$, i. e., 8 and 15 in the first and second considered regimes, respectively.

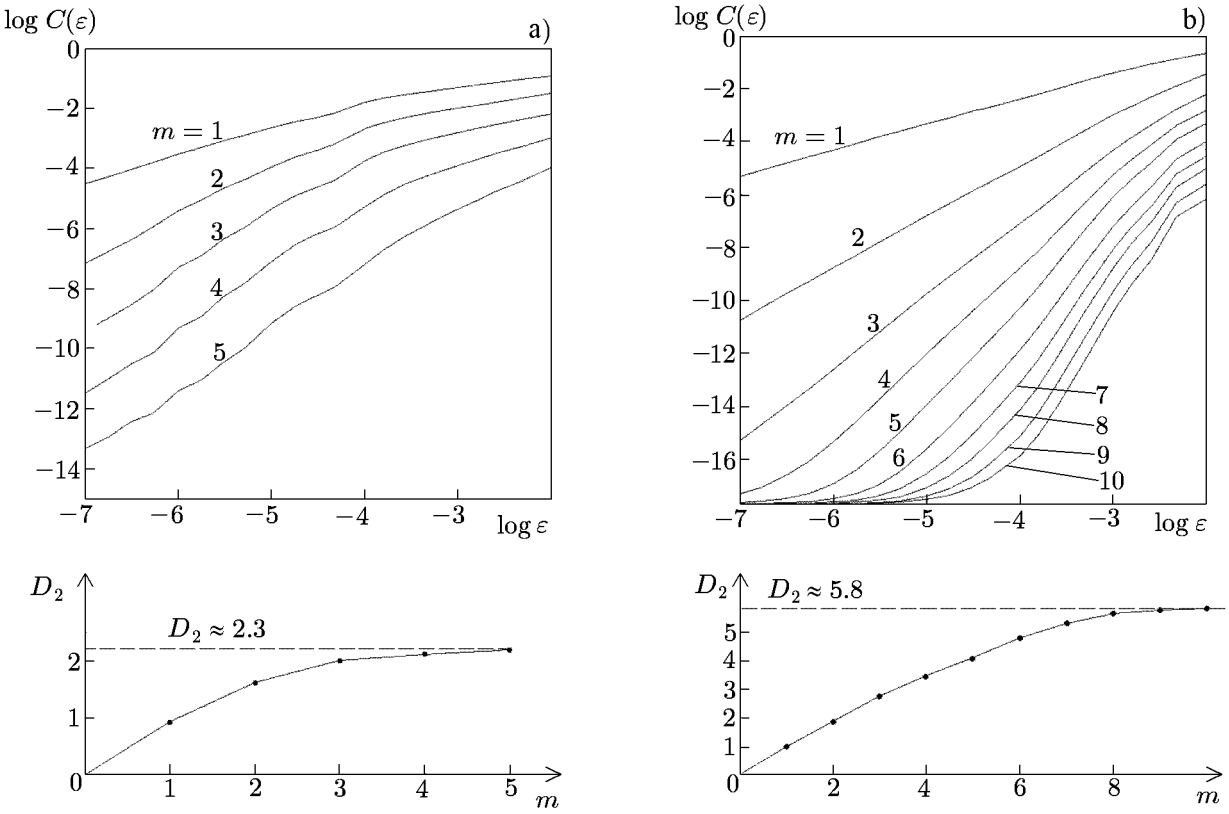


Fig. 11. Diagrams of the dependence of the correlation integral on the resolution scale $\varepsilon$ and the embedding dimension $m$ (top) and the dependence of the estimate of the correlation dimension on $m$ (bottom) based on the scalar time series obtained by numerical solution of Eqs. (1) and (2) in the regime of weak chaos for $L = 4.24$ (*a*) and in the regime of developed chaos for $L = 6.1$ (*b*). The parameters of the algorithm are given in Table 2.

TABLE 2. Parameters of the algorithm used for estimation of the correlation dimension.

| Type of regime | Normalized length | Step of sampling over normalized time | Number of readouts of processed realization | Sampling step of time-series elements during reconstruction of vectors |
|---|---|---|---|---|
| Weak chaos | 4.24 | 5/160 | 74 000 | 6 |
| Developed chaos | 6.1 | 3/100 | 200 000 | 7 |

## 6. CONCLUSIONS

In this paper, the problem of the nature of chaos in a BWO is considered again, focusing at development of an algorithm and calculation of several Lyapunov exponents. It is shown that a developed chaotic regime, observed when the electron-beam current exceeds the starting current by a factor of 30 or greater, must be qualified as hyperchaos since it features the presence of more than one positive Lyapunov exponent. This regime is compared with weak chaos arising for smaller values of the current via a period-doubling cascade of self-modulation. Attention is paid to the difference in the spectral and correlation parameters, the distribution functions, the Lyapunov-exponent spectrum, and the dimensional properties of the attractors.

The appearance of regimes with an increasing number of positive Lyapunov exponents with increase in the nonequilibrium parameter is a typical property of distributed systems to which a BWO belongs. It

should be mentioned that it is exactly hyperchaos regimes that are promising from the viewpoint of using a BWO as an electronically tunable narrow-band noise generator.

Owing to the universal nature of Eqs. (1), the obtained results can be applied for a broad range of electronic devices with long-term backward-wave interaction with the inertial bunching mechanism, including a relativistic BWO, ubitrons and scattrons, gyro-BWO, etc. in certain ranges of the operating parameters.

This work was supported by the Russian Foundation for Basic Research (project No. 03–02–16192) and the Scientific and Educational Center of Nonlinear Dynamics and Biophysics of the Saratov State University (grant REC-006 of CRDF and the Ministry of Education of the Russian Federation). The authors are grateful to B. P. Bezruchko, A. P. Kuznetsov, N. M. Ryskin, and V. N. Titov for the discussion and to I. R. Sataev and E. P. Seleznev for help with the numerical calculations.

**REFERENCES**

1. V. N. Shevchik and D. I. Trubetskov, eds., *Electronics of Backward-Wave Oscillators* [in Russian], Saratov State Univ., Saratov (1975), Ch. III, p. 135.
2. N. S. Ginzburg, S. P. Kuznetsov, and T. N. Fedoseeva, *Radiophys. Quantum Electron.*, **21**, No. 7, 728 (1978).
3. N. S. Ginzburg and S. P. Kuznetsov, in: *Relativistic High-Frequency Electronics. Problems of Increasing the Power and Frequency of Radiation* [in Russian], Inst. Appl. Phys. USSR Acad. Sci., Gorky (1981), p. 101.
4. B. P. Bezruchko, N. S. Ginzburg, and S. P. Kuznetsov, in: *Lectures in Microwave Electronics, Book 5* [in Russian], Saratov State Univ., Saratov (1978), p. 236.
5. B. P. Bezruchko and S. P. Kuznetsov, *Radiophys. Quantum Electron.*, **21**, No. 7, 739 (1978).
6. B. P. Bezruchko, S. P. Kuznetsov, and D. I. Trubetskov, *Sov. Phys. JETP Lett.*, **29**, 162 (1979).
7. B. P. Bezruchko, S. P. Kuznetsov, and D. I. Trubetskov, in: *Nonlinear Waves. Stochasticity and Turbulence* [in Russian], Inst. Appl. Phys. USSR Acad. Sci., Gorky (1988), p. 29.
8. B. P. Bezruchko, L. V. Bulgakova, S. P. Kuznetsov, and D. I. Trubetskov, in: *Lectures in Microwave Electronics and Radiophysics, Book 5* [in Russian], Saratov State Univ., Saratov (1981), p. 25.
9. B. P. Bezruchko, L. V. Bulgakova, S. P. Kuznetsov, and D. I. Trubetskov, *Radio Eng. Electron. Phys.*, **28**, No. 6, 76 (1983).
10. N. S. Ginzburg, N. I. Zaitsev, E. V. Ilyakov, et al., *Phys. Rev. Lett.*, **89**, 108304 (2002).
11. N. S. Ginzburg, N. I. Zaitsev, E. V. Ilyakov, et al., *Tech. Phys. Lett.*, **24**, No. 10, 816 (1998).
12. N. S. Ginzburg, N. I. Zaitsev, E. V. Ilyakov, et al., *Izv. Vyssh. Uchebn. Zaved., Prikl. Nelin. Din.*, **7**, No. 5, 60 (1999).
13. V. A. Balakirev, A. O. Ostrovsky, and Yu. V. Tkach, *Zh. Tekh. Fiz.*, **61**, No. 2, 158 (1991).
14. L. V. Pegel, *Russ. Phys. J.*, **39**, No. 12, 1210 (1996).
15. S. P. Kuznetsov, in: *Proc. Int. Symposium "Topical Problems of Nonlinear Wave Physics," Nizhny Novgorod, Russia, Sept. 6–12, 2003*, p. 78.
16. R. Sh. Amirov, B. P. Bezruchko, V. A. Isaev, and A. P. Chetverikov, in: *Lectures in Microwave Electronics and Radiophysics, Book 5* [in Russian], Saratov State Univ., Saratov (1983), p. 90.
17. V. A. Kats, "Stochastic self-oscillations in electronic distributed systems at ultrahigh frequencies," Ph.D. Thesis [in Russian], Saratov State Univ., Saratov (1985).
18. B. Levush, T. N. Antonsen, A. Bromborsky, et al., *IEEE Trans. Plasma Sci.*, **20**, No. 3, 263 (1992).

19. S. A. Astakhov, B. P. Bezruchko, A. V. Zborovsky, and D. I. Trubetskov, in: *Proc. Int. Sci. Techn. Conf. "Topical Problems in Electronic Instrument Engineering," Vol. 1* [in Russian], Saratov State Technical Univ., Saratov (1998), p. 39.
20. N. M. Ryskin and V. N. Titov, *Radiophys. Quantum Electron.*, **44**, No. 10, 793 (2001).
21. A. E. Khramov, *Tech. Phys. Lett.*, **29**, No. 6, 467 (2003).
22. A. A. Koronovsky and A. E. Khramov, *Tech. Phys. Lett.*, **29**, No. 6, 510 (2003).
23. N. M. Ryskin, V. N. Titov, and D. I. Trubetskov, *Doklady Physics*, **43**, No. 2, 90 (1998).
24. N. M. Ryskin and V. N. Titov, *Izv. Vyssh. Uchebn. Zaved., Prikl. Nelin. Din.*, **6**, No. 1, 75 (1998).
25. B. P. Efimov, B. Ya. Krivitsky, K. A. Lukin, et al., in: *The Millimeter- and Submillimeter-Wave Electronics. Collection of Papers* [in Russian], Naukova Dumka, Kiev (1988), p. 68.
26. V. A. Rakityansky, in: *Radiophysics and Electronics. Collection of Papers* [in Russian], Inst. Radiophys. Electron. Nat. Acad. Sci. Ukraine, Kharkov (1997), Vol. 2, No. 1, p. 111.
27. M. Feigenbaum, *Usp. Fiz. Nauk*, **141**, No. 2, 343 (1983).
28. H. Shuster, *Deterministic Chaos. An Introduction*, Physik-Verlag, Weinheim (1984).
29. S. P. Kuznetsov, *Dynamic Chaos* [in Russian], Nauka, Moscow (2001).
30. P. Berge, Y. Pomeau, and C. Vidal, *Order in Chaos*, Wiley, New York (1984).
31. G. Benettin, L. Galgani, and J.-M. Strelcyn, *Phys. Rev. A*, **14**, 2338 (1976).
32. G. Benettin, L. Galgani, A. Giorgilli, and J.-M. Strelcyn, *Meccanica*, **15**, 9 (1980).